Extending the wind profile much higher than the surface layer

Pena Diaz, Alfredo; Gryning, Sven-Erik; Hasager, Charlotte Bay; Courtney, Michael

Published in:
EWEC 2009 Proceedings online

Publication date:
2009

Document Version
Publisher's PDF, also known as Version of record

Extending the wind profile much higher than the surface layer

Alfredo Peña, Sven-Erik Gryning,
Charlotte Bay Hasager, and Michael Courtney
Wind Energy Division,
Risø National Laboratory for Sustainable Energy, DTU
alfredo.pena.diaz@risoe.dk

Abstract:

The wind speed profile over flat and homogeneous terrain has been measured by combining cup anemometer and lidar observations at Høvsøre, Denmark. The comparison between the cup anemometer and the lidar measurements show good agreement up to 160 m, the highest level of the instruments at the site. However, lidar wind profiles are available up to 300 m. Models for the wind speed profile have been derived using mixing-length theory and are in good agreement with the observations. These have been classified into a wide range of stability classes based on atmospheric turbulence measurements close to the ground.

Keywords: Atmospheric boundary layer, homogeneous terrain, lidar, mixing length, surface layer, stability, wind profiles

1 Introduction

The National Test Station for Wind Turbines at Høvsøre, Denmark, provides the opportunity to study the wind speed profile over homogenous terrain, due to the flat area observed within a wide upwind sector (approx. $90°$). At the site, a heavily instrumented meteorological mast and two light towers have been observing wind speed, wind direction, and turbulence continuously for the last four years. This has allowed the study of many climatologic features, as well as the description of the wind speed profile up to 160 m, where the highest cup and sonic anemometers are installed.

New parameterizations of the wind profile for flow in the entire atmospheric boundary layer (ABL) were developed by [1] based on mixing-length theory and these compared well with the climatologic Høvsøre data within the flat upwind sector. The model and the measurements showed the need for parameterizations that take into account the boundary-layer height and for an improvement of models of the length scale, in order to predict more accurately the wind speed. This is because the estimations based on the traditional surface-layer scaling start to deviate from the measurements as shown over land in [1] and over the sea in [2], e.g. at heights $40 - 60$ m under very stable conditions, which are current wind turbine operating heights. Large deviations were also found by [1] in near-neutral conditions at heights $116 - 160$ m where the large wind turbines operate.

In this study, we have observed the wind profile in detail up to 300 m, i.e. much higher than the surface layer ($\approx 10\%$ of the ABL), under different atmospheric stability conditions using combined lidar/cup anemometer observations at Høvsøre. The lidar technology was successfully used for wind profiling over land, e.g. as shown in [3] and [4], and over the sea, e.g. in [2] and [5]. The lidar observations are then used to extend the wind speed profiles up to 300 m from the cup anemometer observations. We use the classical mixing-length model in [6] for the derivation of new wind profiles for different atmospheric stabilities. The model for the wind profile accounts for the effect of the boundary-layer height that is estimated to be within the range of measurements during this period. Moreover, the mixing-length concept was successfully used to correct the wind speed profile for diabatic conditions using Monin-Obukhov Similarity theory (MOST) ([7]) within the surface layer.

2 Theory

From mixing-length theory ([6], [8]), the mean wind shear in the ABL, $\partial U/\partial z$, can be derived as

$$\frac{\partial U}{\partial z} = \frac{u_*}{\ell} \tag{1}$$

where U is the magnitude of the horizontal wind vector ($U^2 = u^2 + v^2$, u and v being the wind speed components in the x and y directions, respectively), z is the height above ground, u_* is the local friction velocity, and ℓ is the local mixing

length. To account for the effect of the boundary-layer height, z_i, the friction velocity is modeled to decrease with height as shown in [1] and [9]:

$$u_* = u_{*o}\left(1 - \frac{z}{z_i}\right) \tag{2}$$

where u_{*o} is the surface-layer friction velocity. We use the mixing-length model proposed by [6]:

$$\ell = \frac{\kappa z}{1 + \frac{\kappa z}{\lambda}} \tag{3}$$

where κ is the von Kármán constant and λ is the value of length scale reached by ℓ in the free atmosphere. λ was estimated by [6] under neutral and barotropic conditions to be equal to $\lambda = 0.00027G/f_c$ where G and f_c are the geostrophic wind magnitude and the Coriolis parameter, respectively, based on the reanalysis of the Leipzig wind profile in [10].

Following the analysis from [1] for their proposed length scale, the mixing length in Eq. (3) can be rewritten as

$$\frac{1}{\ell} = \frac{1}{\kappa z} + \frac{1}{\lambda} \tag{4}$$

where the term $1/\kappa z$ corresponds to the inverse of the traditional surface-layer length scale. [7] corrected the behavior of the surface-layer wind shear, the base of MOST, to account for the stability of the atmosphere and found a non-dimensional parameter,

$$\phi_m = \frac{\kappa z}{u_{*o}}\frac{\partial U}{\partial z} \tag{5}$$

where ϕ_m is the dimensionless wind shear. Empirical relationships (the so-called flux-profile relationships) of the form:

$$\phi_m = \left(1 - a\frac{z}{L}\right)^p \qquad \text{and} \tag{6}$$

$$\phi_m = 1 + b\frac{z}{L} \tag{7}$$

were found by [11] and [12] to fit well data for unstable and stable conditions, respectively. a, b, and p are fitted constants from the different experiments ([11] fitted $a = 15$, $b = 4.7$, and $p = -1/4$ and [12] $a = 19.3$, $b = 6$, and $p = -1/4$) and L is the Obukhov length,

$$L = -\frac{{u_{*o}}^3 T_o}{\kappa g \overline{w'\Theta_v{}'}_o} \tag{8}$$

where T_o is the mean surface-layer temperature, g is the gravitational acceleration and $\overline{w'\Theta_v{}'}_o$ is the surface-layer kinematic heat flux.

Thus, correcting the surface-layer length scale in Eq. (4) using the ϕ_m function as in Eq. (5) and using Eq. (2) for the friction velocity, the mean wind shear is then given by:

$$\begin{aligned}\frac{\partial U}{\partial z} &= u_{*o}\left(1 - \frac{z}{z_i}\right)\left(\frac{1}{\kappa z}\phi_m + \frac{1}{\lambda}\right), \\ &= \underbrace{\frac{u_{*o}}{\kappa z}\phi_m}_{\text{I}} - \underbrace{\frac{u_{*o}}{\kappa z_i}\phi_m}_{\text{II}} + \underbrace{\frac{u_{*o}}{\lambda}}_{\text{III}} - \underbrace{\frac{u_{*o}}{\lambda}\frac{z}{z_i}}_{\text{IV}}.\end{aligned} \tag{9}$$

The integration with height of the term I in Eq. (9) gives:

$$U = \frac{u_{*o}}{\kappa}\left[\ln\left(\frac{z}{z_o}\right) - \psi_m\right] \tag{10}$$

where ψ_m is the diabatic correction to the logarithmic wind profile, which is a function of a, b, p, and z/L as shown in [13]. Eq. (10) is the traditional surface-layer wind profile that predicts well the wind behavior close to the surface as shown over land, e.g. in [1] and [14], and over the sea, e.g in [2] and [15].

The integration with height of the term II in Eq. (9) depends on the stability condition, therefore, using Eqs. (6) and (7):

$$U = \frac{u_{*o}}{\kappa}\frac{(-L + az)\,(1 - az/L)^p + L}{z_i a\,(1 + p)} \tag{11}$$

$$U = \frac{u_{*o}}{\kappa}\left(\frac{z}{z_i} + \frac{b}{2L}\frac{z^2}{z_i}\right) \tag{12}$$

for unstable and stable conditions, respectively. For unstable conditions and small values of z/L, Eq. (11) is approximated as

$$U = \frac{u_{*o}}{\kappa}\frac{z}{z_i}. \tag{13}$$

The integration with height of the terms III and IV in Eq. (9) results in, respectively,

$$U = \frac{u_{*o}}{\kappa}\left(\frac{\kappa z}{\lambda}\right) \qquad \text{and} \tag{14}$$

$$U = \frac{u_{*o}}{\kappa}\left(\frac{\kappa z}{\lambda}\frac{z}{2z_i}\right). \tag{15}$$

The wind profile taking into account all terms is then given for unstable conditions as

$$U = \frac{u_{*o}}{\kappa}\left[\ln\left(\frac{z}{z_o}\right) - \psi_m + \frac{\kappa z}{\lambda}\left(1 - \frac{z}{2z_i}\right) - \frac{z}{z_i}\right], \tag{16}$$

for stable conditions as

$$\begin{aligned}U &= \frac{u_{*o}}{\kappa}\left[\ln\left(\frac{z}{z_o}\right) + b\frac{z}{L}\left(1 - \frac{z}{2z_i}\right)\right] \\ &\quad + \frac{u_{*o}}{\kappa}\left[\frac{\kappa z}{\lambda}\left(1 - \frac{z}{2z_i}\right) - \frac{z}{z_i}\right],\end{aligned} \tag{17}$$

and for neutral conditions, i.e. $\phi_m = 1$ in Eq. (9), as

$$U = \frac{u_{*o}}{\kappa}\left[\ln\left(\frac{z}{z_o}\right) + \frac{\kappa z}{\lambda}\left(1 - \frac{z}{2z_i}\right) - \frac{z}{z_i}\right]. \tag{18}$$

Figure 1 (left panel) illustrates the behavior of the length scale model compared to the traditional surface-layer length scale for unstable, neutral, and stable conditions. It is shown that the value of λ limits the surface-layer length scale for all stability conditions. In Figure 1 (right panel) is shown the effect of the model on the wind speed profile where the wind speed is well predicted by the surface-layer wind profile up to $z \leq 0.1 z_i$ and, then, deviates predicting higher wind speeds at higher altitudes in stable conditions and lower wind speeds in neutral and unstable conditions.

The boundary-layer height can be estimated using the Rossby-Montgomery formula in [16] for neutral conditions as

$$z_i = C \frac{u_{*o}}{|f_c|} \tag{19}$$

where C is a rather fluctuating value. For the stable cases, z_i is also computed using Eq. (19), although it takes into account the contribution of mechanical turbulence only. Eq. (19) was found to be useful for boundary-layer height determination as shown in [2] for wind profiles that showed a systematic decrease in friction velocity, the closer the conditions were to stable atmospheres. For the unstable cases, there are not suitable diagnostic equations for z_i, therefore, it is roughly approximated using ceilometer data, as will be shown in Section 4.

3 Site and measurements

Measurements of the wind profile as well as the meteorological parameters were performed at the National Test Station for Wind Turbines at Høvsøre, Denmark. The Test Station is located in a rural area close to the west coast of Jutland (Figure 2). The analysis regards to an upwind land area from the view of the meteorological mast, i.e. for wind directions between $30^\circ - 125^\circ$, where the terrain is flat and homogeneous and the wind is not influenced by the water/land discontinuities or the wind turbines north of the mast.

A Leosphere WindCube® lidar was installed few meters from the meteorological mast at Høvsøre during the period 6 July 2008–26 October 2008 performing measurements of wind speed and direction at 10 heights: 40, 60, 80, 100, 116, 130, 160, 200, 250, and 300 m. Technical details about the lidar and the measurement technique are given in [17]. Measurements from the cup and sonic anemometers installed at the mast as well as the lidar were stored as 10-min averages. Only wind speeds above 2 m s^{-1} are used and the wind sector is selected based on the observation from a wind vane at 10 m.

The atmospheric conditions are selected based on estimation of the Obukhov length, Eq. (8), from turbulent fluxes observed with a sonic anemometer at 10 m. The measurements are classified in different atmospheric classes within intervals of Obukhov length as shown in Table 1.

Obukhov length interval [m]	Atmospheric stability class
$10 \leq L \leq 50$	Very stable (vs)
$50 \leq L \leq 200$	Stable (s)
$200 \leq L \leq 500$	Near stable (ns)
$\lvert L \rvert \geq 500$	Neutral (n)
$-500 \leq L \leq -200$	Near unstable (nu)
$-200 \leq L \leq -100$	Unstable (u)
$-100 \leq L \leq -50$	Very unstable (vu)

Table 1: Stability classes according to Obukhov length, L.

The lidar observations compare well with the measurements of the cup anemometers at the meteorological mast and light tower. In Figure 3, this comparison is illustrated for the two higher cup anemometers at 116 m (at the meteorological mast) and 160 m (at the light tower) and the corresponding lidar observations at the same heights. Similar results (not shown) were found for the other lidar/cup overlapping heights at 40, 60, 80, and 100 m. Thus, we combine the cup anemometer with the lidar observations. Each 10-min wind profile up to 116 m corresponds to the cup anemometer observations (10, 40, 60, 80, 100, and 116 m) and it is extended up to 300 m with the lidar measurements (130, 160, 200, 250, and 300 m).

4 Results

All combined lidar/cup 10-min wind profiles are classified according to the stability classes in Table 1. The boundary-layer height is estimated using Eq. (19) with $C = 0.15$ for neutral and near stable conditions based on the fittings of z_i by [1] and the original estimation of C in [16]. For stable and very stable conditions, lower values are used, $C = 0.12$ and $C = 0.10$, respectively. A decreasing C is chosen based on the observation of low-level jets under very stable conditions at heights around 100 m. A value $C = 0.10$ was also used by [2] for stable conditions. For unstable conditions, aerosol concentrations are analyzed using observations from a Vaisala CL31 ceilometer installed close to the meteorological mast. The selected upwind sector is one of the less predominant at Høvsøre, therefore, the observations are narrowed

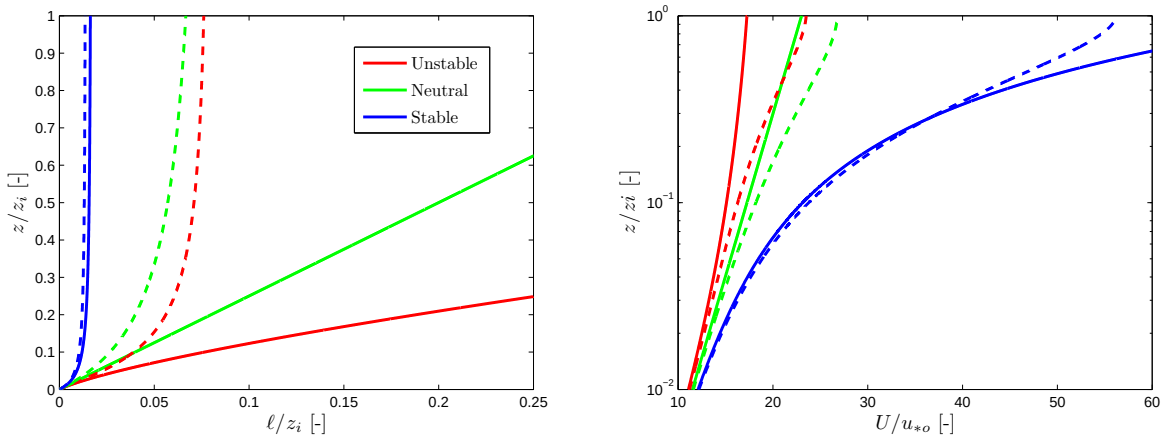

Figure 1: Profiles of mixing length (left panel) and wind speed (right panel) in the ABL for different stability conditions. The length scale model, $1/\ell = \phi_m/(\kappa z) + 1/\lambda$, is shown in dashed lines and the surface-layer length scale, $1/\ell = \phi_m/(\kappa z)$, in solid lines. The wind profile models, Eqs. (16)–(18), shown in dash lines and the predictions using the traditional surface-layer wind profile, Eq. (10), in solid lines are computed using $\kappa = 0.4$, $L = 200$ and $L = -200$ m for stable and unstable conditions, respectively, $z_o = 0.1$ m, $\lambda = 80$ m for all stability conditions, $p = -1/3$, $a = 12$, and $b = 4.7$.

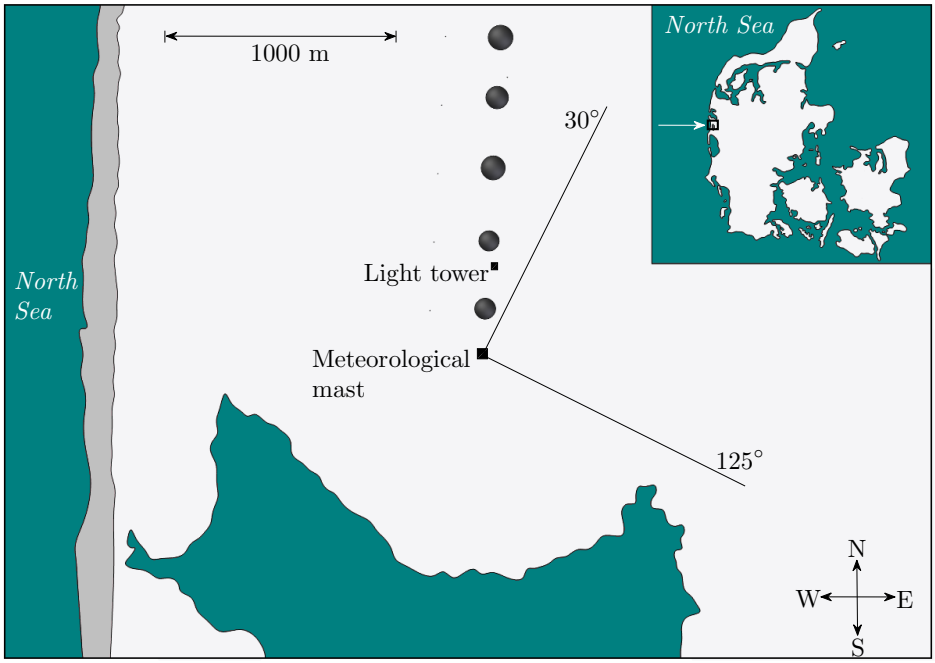

Figure 2: National Test Station for Wind Turbines at Høvsøre, Denmark. The position of the meteorological mast ($56°26'26''$N, $8°9'3''$E) and light tower in rectangles, and the wind turbines in circles is indicated. In the top-right corner is shown the location of Høvsøre in Denmark. The blue color indicates water and the white land surface.

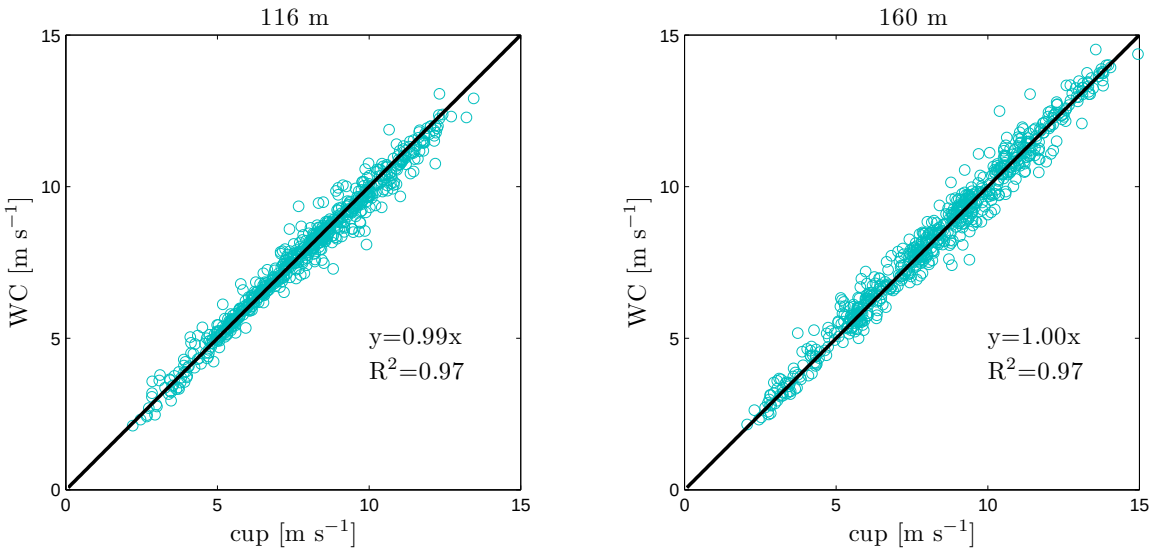

Figure 3: Comparison of horizontal 10-min wind speeds between the lidar (WC) and the cup anemometers at two overlapping heights, 116 and 160 m. A linear regression forced to the origin is performed. The correlation coefficient, R^2, is also given.

in specific days. In particular, on the 23 and 24 September 2008, the wind was continously blowing from the north-easterly sectors where 40% of the 10-min observations of all unstable classes are found. The evolution of aerosol backscatter based on ceilometer observations for these days is illustrated in Figure 4. The scale is normalized in order to see clearly the aerosol backscatter daily evolution, due to the presence of clouds at midday that highly enhance the measurements. The very unstable profiles are observed at $0900-1500$ local standard time (LST), unstable profiles at $0830-1000$ and $1500-1600$ LST, and near unstable profiles at $0800-0830$ and $1600-1630$ LST. A higher value for z_i is expected for the very unstable conditions and according to Figure 4, high concentrations of aerosol are found for both days between $0900-1500$ LST at $600-700$ m. Thus, we assume $z_i = 650$ m for very unstable conditions, and $z_i = 600$ and 550 m for unstable and near unstable conditions, respectively.

The mean meteorological parameters computed in each stability class are given in Table 2. A comparison with a longer (approx. four year) measurement period at Høvsøre in [1] shows that the mean parameters agree well for all stability conditions. The higher differences are found in the estimation of the roughness length that is around three times higher for this dataset, which is expected for summer periods. z_o is estimated from Eq. (10) using the observations at 10 m from the cup anemometer wind speed and the sonic anemometer turbulent fluxes.

A comparison between the combined cup/lidar observations and the predicted profiles using the traditional surface-layer wind profile, Eq. (10), is illustrated in Figure 5. A mean low-level jet for the very stable condition is observed at around 100 m, thus, the boundary-layer height is estimated at this height. The predicted wind profiles fit well the observations within the surface layer that extends up to approx. 65, 50, and 10 m, for very unstable, neutral, and very stable conditions, respectively. Above the surface layer, the predicted wind profile underestimates the wind speed up to 300 m, except for the very stable case that overestimates it at $40-60$ m.

Stability class	L [m]	u_{*o} [m s^{-1}]	z_o [m]	z_i [m]	No. of Profiles
vs	27	0.13	0.006	105	75
s	115	0.25	0.027	251	143
ns	321	0.35	0.034	434	125
n	2771	0.40	0.045	498	104
nu	-334	0.39	0.047	550*	61
u	-143	0.41	0.046	600*	63
vu	-74	0.38	0.044	650*	45

Table 2: Computed mean parameters in each atmospheric stability class. *The values for z_i in unstable conditions are estimated using the ceilometer data.

Using the wind speed measurements and the mean parameters in Table 2, we fit the value of λ from the wind profile models, Eqs. (16)–(18), for each stability class. These are given in Table 3.

A comparison between the combined cup/lidar observations and the predicted profiles using the new wind profile models, Eqs. (16)–

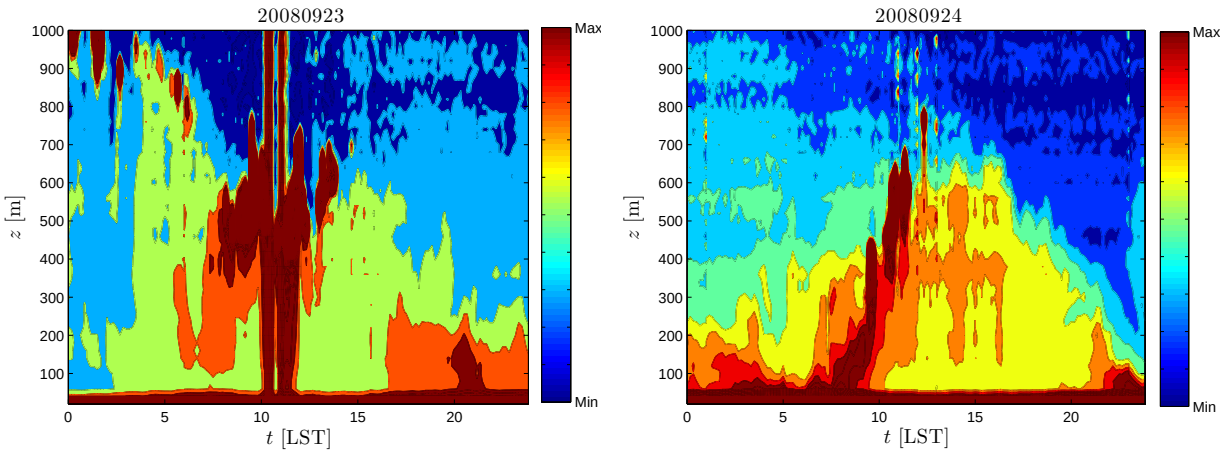

Figure 4: Ceilometer observations of normalized aerosol backscatter on the 23 September 2008 (left panel) and 24 September 2008 (right panel). In the t-axis, local standard time (LST) is given.

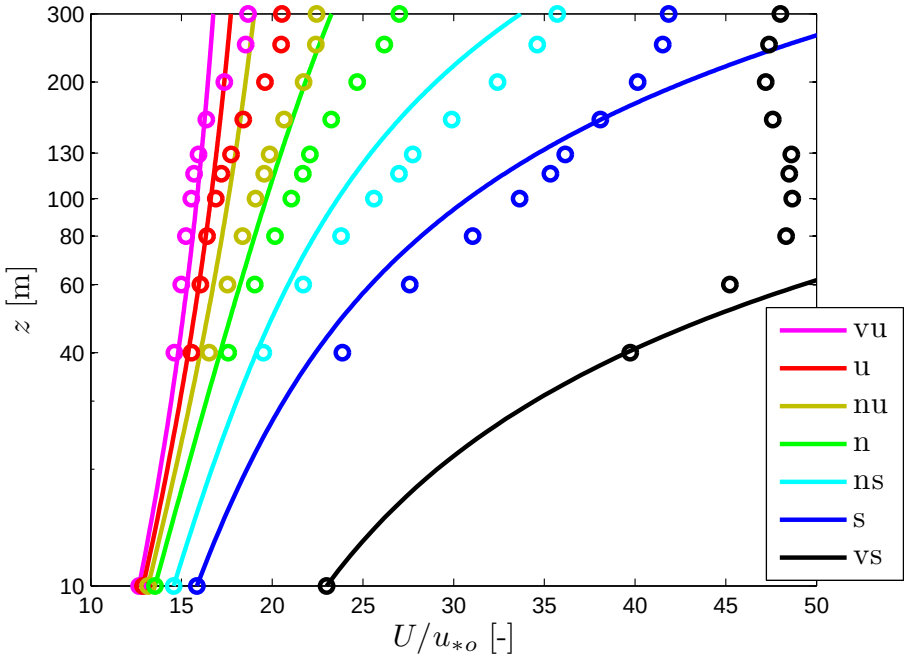

Figure 5: Comparison of combined lidar/cup observations, in markers, and the predictions from the traditional surface-layer wind profile, Eq. (10) in solid lines, for each atmospheric stability class using $a = 12$, $b = 4.7$, $p = -1/3$, $k = 0.4$, and the values in Table 2. The legend is given in relation with Table 1.

Stability class	vu	u	nu	n	ns	s	vs
λ [m]	168	81	55	39	26	15	10

Table 3: Computed value of λ for each stability class.

(18), is illustrated in Figure 6. The predicted wind profiles are shown until they reach the computed/estimated boundary-layer height, marking the limit of their validity. For very unstable and unstable conditions, the wind profile model agrees well with the observations showing a low overestimation of the wind speed from $60 - 130$ m, but correcting for the over-speeding of the observations at around 160 m. For the rest of stability classes, the predictions agree well with the measurements, correcting the underestimations of the traditional surface-layer wind profile.

5 Conclusions

New parameterizations of the wind speed profile for flow in the entire ABL over homogeneous and flat terrain were derived for different atmospheric stability conditions, using the classical mixing-length scale formulation in [6]. These new wind speed profiles account for the effect of the boundary-layer height, which is normally neglected in wind engineering calculations. The models were in good agreement with the observations up to 300 m and corrected the under- and over-estimation of the wind speed of the traditional wind profile beyond surface layer.

The comparison of horizontal wind speed between the cup anemometers and the lidar measurements showed good agreement up to 160 m, the highest level of the instruments. The lidar instrument was found to be useful for the extension of the wind profile from cup anemometers observations at the tall meteorological mast at Høvsøre.

The boundary-layer height was computed from surface-layer turbulence parameters in neutral and all stable conditions using the Rossby-Montgomery formula. This, in particular, estimates a boundary-layer height close to the height where low-level jets were observed in very stable conditions. Ceilometer data was found to be useful to roughly estimate the height of the unstable boundary layer from the backscatter of the aerosols.

Acknowledgments

The authors would like to thank the Test and Measurements Program of the Wind Energy Division at Risø DTU for the acquisition of the data. Funding from The Danish Council for Strategic Research to the project "12 MW" Sagsnr. 2104-05-0013 is also acknowledged. I (AP) would like to thank Henrik Søgaard from the University of Copenhagen for the supervision of my PhD study.

References

[1] S.-E. Gryning, E. Batchvarova, B. Brümmer, H. Jørgensen, and S. Larsen. On the extension of the wind profile over homogeneous terrain beyond the surface layer. *Boundary-Layer Meteorol.*, 124:251–268, 2007.

[2] A. Peña, S-E. Gryning, and C. B. Hasager. Measurements and modelling of the wind speed profile in the marine atmospheric boundary layer. *Boundary-Layer Meteorol.*, 129:479–495, 2008.

[3] J. Mann, E. Dellwik, F. Bingöl, and O. Rathmann. Laser measurements of flow over a forest. *J. Phys.: Conf. Ser.*, 75:012057 (7 pp), 2007.

[4] D. Kindler, A. Oldroyd, A. MacAskill, and D. Finch. An eight month test campaign of the qinetiq zephir system: Preliminary results. *Meteorol. Zeitschrift*, 16(5):479–489, 2007.

[5] A. Peña, C. B. Hasager, S.-E. Gryning, M. Courtney, I. Antoniou, and T. Mikkelsen. Offshore wind profiling using light detection and ranging measurements. *Wind Energy*, in Press, 2008.

[6] A. K. Blackadar. The vertical distribution of wind and turbulent exchange in a neutral atmosphere. *J. Geophys. Res.*, 67:3095–3102, 1962.

[7] A. S. Monin and A. M. Obukhov. Osnovnye zakonomernosti turbulentnogo peremeshivanija v prizemnom sloe atmosfery (Basic laws of turbulent mixing in the atmosphere near the ground). *Trudy Geofiz. Inst. AN SSSR*, 24(151):163–187, 1954.

[8] L. Prandtl. Meteorologische Anwendung der Strömungslehre (Meteorological application of fluid mechanics). *Beitr. Phys. Atmos.*, 19:188–202, 1932.

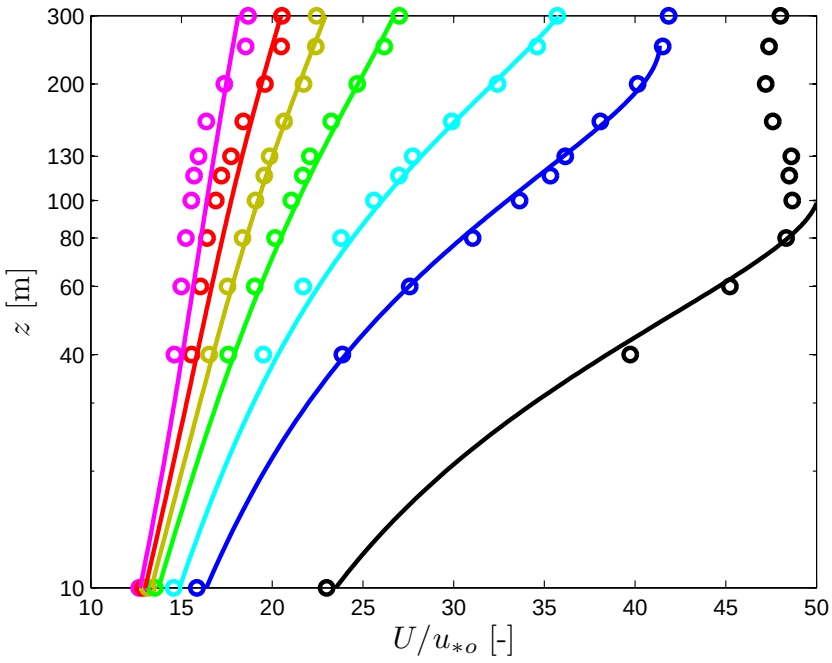

Figure 6: Comparison of combined lidar/cup observations, in markers, and the predictions from the wind profile models, Eqs. (16)–(18) in solid lines, for each atmospheric stability class (in colors as in Figure 5) using $a = 12$, $b = 4.7$, $p = -1/3$, $k = 0.4$, and the values in Table 2 and Table 3.

[9] H. A. Panofsky. *Tower Micrometeorogy. In: Haugeb DA (ed) Workshop on Micrometeorolgy*. American Meteorology Society, 1973.

[10] H. Lettau. A re-examination of the "Leipzig wind profile" considering some relations between wind and turbulence in the frictional layer. *Tellus*, 2:125–129, 1950.

[11] J. A. Businger, J. C. Wyngaard, Y. Izumi, and E. F. Bradley. Flux-profile relationships in the atmospheric surface layer. *J. Atmos. Sci.*, 28:181–189, 1971.

[12] U. Högström. Non-dimensional wind and temperature profiles in the atmospheric surface layer: a re-evaluation. *Boundary-Layer Meteorol.*, 42:55–78, 1988.

[13] R. B. Stull. *An introduction to boundary layer Meteorology*. Kluwer Academic Publishers, 1988.

[14] D. M. Carl, T. C. Tarbell, and H. A. Panofsky. Profiles of wind and temperature from towers over homogeneous terrain. *J. Atmos. Sci.*, 30:788–794, 1973.

[15] A. Peña and S.-E. Gryning. Charnock's roughness length model and non-dimensional wind profiles over the sea. *Boundary-Layer Meteorol.*, 128:191–203, 2008.

[16] C. G. Rossby and R. B. Montgomery. The layers of frictional influence in wind and ocean currents. *Pap. Phys. Oceanogr. Meteorol.*, 3(3):101 pp, 1935.

[17] M. Courtney, R. Wagner, and P. Lindelöw. Testing and comparison of lidars for profile and turbulence measurements in wind energy. *Earth Environ. Sci.: Conf. Ser.*, 1:012021 (14 pp), 2008.